Investigation of a Cascaded H-bridge Photovoltaic Inverter under non-Uniform Insolation Conditions by Hardware-in-the-Loop Test

Hossein Iman-Eini[1], Sarath Tennakoon[2]

[1] School of Electrical and Computer Engineering, Faculty of Engineering, University of Tehran, Tehran, Iran

[2]Faculty of Computing, Engineering, and Sciences, Staffordshire University, Stoke-on-Trent, UK

Corresponding author email: imaneini@ut.ac.ir

Abstract- In this paper, the cascaded H-bridge (CHB) multilevel inverter is employed as a grid connected inverter. This kind of inverter has interesting features compared to conventional inverters, including better efficiency, lower THD, lower common mode current injection, and better waveform quality. Using a series connection of H-bridge cells in this topology, a high modularity is achieved and a stepwise voltage waveform is synthesized at the ac side, leading to lower filter size and complexity. This topology processes the electric power in one stage and does not need any step-up voltage transformer for grid connection. The dynamic performance of control system is studied through simulations and is compared with the conventional approach. In addition, a new voltage estimation approach is proposed to reduce the number of voltage sensors compared to existing methods. The simulation results are presented for a 1.5 kW grid connected 7-level CHB inverter and then the hardware-in-the-loop implementation of the CHB inverter is presented to verify the performance of control system.

Keywords- Cascaded H-bridge Inverter, Grid Connection, Hardware-in-the-loop implementation, Photovoltaics, and Real-time simulation.

1- Introduction

Recently the increasing demand for electric power and the reduction in fossil fuels have led to more interest on renewable energies. Among the renewables, the solar energy is easily accessible and can be readily converted to the electric power by photovoltaic (PV) panels [1]. The photovoltaic energy conversion does not employ any rotating parts, and therefore, its lifetime is long and the maintenance cost is low. This technology however needs high initial investment for PV panels, inverter, mechanical structure, and installation. To compensate part of this investment, high efficiency inverters should be employed which bring higher electric power and benefits during the life time of photovoltaic system.

The conventional grid connected inverters employ two stages of power converters for photovoltaic applications [2]. The first stage is a dc/dc boost converter which is connected to the PV panel and tries to extract the maximum power from PV panels. The next stage is a voltage source converter which tries to transfer the electric power into the grid at unity power factor. This kind of PV inverter, however, will lead to higher losses and complexity compared to single stage inverters due to insertion of dc/dc converters [3].

Among different topologies for single stage PV inverters, the cascaded H-bridge multilevel inverter has gained a lot of attention in industry. This topology provides separate dc links which allows independent control of PV arrays, a very interesting feature for improving the efficiency of PV inverter under non-uniform (or partial shading) insolation conditions [4]. In this kind of inverter, the output transformer can be eliminated and the lower switching frequency can

be employed, leading to higher efficiency. Moreover, by synthesizing a step-wise voltage waveform at the ac side, lower THD and common mode current is generated. These features besides the modularity of CHB structure make it an ideal choice for high efficiency and high performance photovoltaic systems [5].

The CHB converter is a multi-input single-output system which has a complex control system when the operating condition of distinct PV arrays (or H-bridge cells) is different [6]. Reference [7] has employed an FPGA based fuzzy control system to control the CHB inverter. The proposed system, however, has not been evaluated under asymmetric operating conditions. In [8], n+1 control loops are employed for a 2n+1 level CHB inverter: *n* of them are used to adjust the capacitor voltage in each dc link, and the other one is necessary for the generation of a sinusoidal input current with unity power factor. In this method, which is known as "conventional control system", the references of dc link voltages are defined through individual MPPT blocks and the current is controlled using a PI controller. Reference [9] uses a similar control method as [8], but it adds a feedforward term to the modulation index of H-bridge cells to compensate their offsets due to unequal operating conditions. Reference [10] has reduced the number of necessary sensors in the CHB inverter. The update frequency of MPPT algorithm, however, has been limited to 1 Hz which limits its usage in many applications. All above references fail to operate correctly when the inverter faces with heavy mismatching conditions.

A few methods have been presented in the literature to control the CHB based PV system under heavy mismatching condition, i.e., an operating condition in which over modulation occurs. Ref. [11] and [12] use reactive po wer compensation (or power factor variable) to stabilize the system. But, an uncontrolled amount of reactive power injection (or absorption) may not be acceptable from a power dispatcher's point of view. Ref. [13] uses a combination of reactive power compensation and a modified level-shifted pulse-width modulation (LS-PWM) to extend the operating range of CHB inverter. This reference, however, uses a two-stage power conversion system which results in higher conversion losses and lower efficiency. In [14], a hybrid modulation technique is used along with a derivative-of-power based control method to use CHB cells up to their full potential and to stabilize single-stage CHB inverters under severe mismatching conditions. The implementation of this method, however, has difficulties due to adoption of derivative term of PV power. Reference [15] has proposed to shift the operating point of H–bridge cells when they incur to the over modulation range due to unequal operating conditions. The proposed technique, however, is limited to a CHB inverter with three H-bridge cells and it does not provide any experimental validation. Reference [16] uses the same idea in [15] and provides experimental results.

Another challenging issue in the CHB based PV inverters is related to the test of control system under different operating conditions. Providing the desired test condition in real environment, however, is so difficult and costly. A reasonable way to overcome this challenge is the hardware-in-the-loop (HIL) simulation of the photovoltaic system by a real-time simulator, e.g., OPAL-RT. This technique allows the user to adjust the test conditions (i.e., irradiance level or temperature of PV arrays) by the software tool [16]. References [17], [18] have just performed the real-time HIL simulation of a simple PV inverter and there is no reference on the HIL implementation of a CHB inverter and its verification under non-uniform insolation conditions.

In this paper, the presented controller in [15] is employed as the basis of control system and is generalized for a CHB inverter with an arbitrary number of H-bridge cells. After presenting the control system and the proposed action under non-uniform insolation conditions, a new estimation method is proposed to calculate the voltage of PV arrays with only one sensor and reducing the number of voltage sensors in contrast to previous approaches. Moreover, the dynamic performance of control system is studied through simulations and is compared with the conventional approach.

The other contribution is related to the implementation of control system by a DSP controller and its insertion in the hardware-in-the-loop structure, where the PV arrays and the CHB inverter will be modeled by the software tool. Using the OPAL-RT simulator, the whole system is simulated in a real-time basis. Using this capability, a desired test condition can be provided for the test of controller; otherwise, a lot of time and cost should be spent for evaluation of control system.

2- Structure of CHB based Photovoltaic Inverter

As it is shown in Fig.1, the CHB inverter consists of *n* series connected H-bridge cells with an inductor located between the inverter and the grid. The dc link of each H-bridge cell is connected to a separate PV array and the ac terminals are connected in series. The total ac terminal voltage can be written as

$$v_{ab} = \sum_{j=1}^{N} v_{hj} \qquad (1)$$

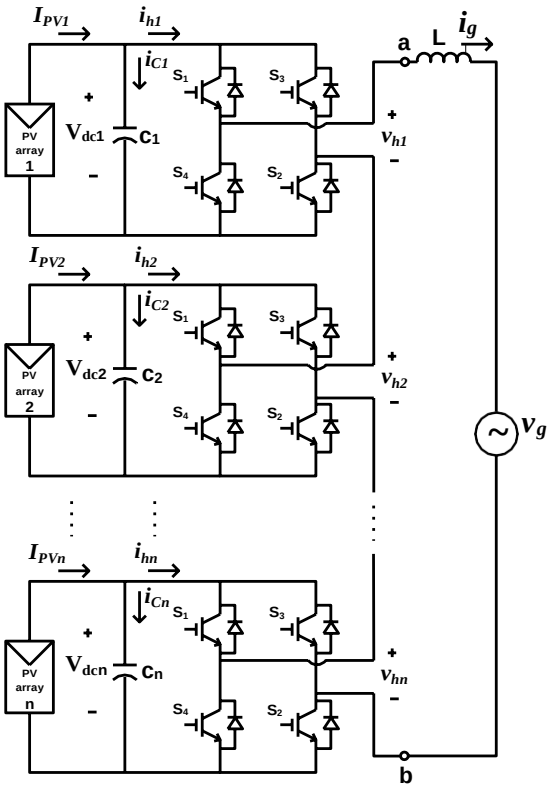

Fig.1. Structure of grid connected CHB inverter

where in (1), v_{hj} is the ac terminal voltage of jth cell and v_{ab} is the total ac terminal voltage. The relation between the dc link voltage and the ac terminal voltage at the jth H-bridge cell is defined by

$$v_{hj}^{1} = s_j \times V_{dcj} \qquad (2)$$

where V_{dcj} is the dc link voltage, v_{hj}^1 represents the first harmonic of ac terminal voltage and s_j is the modulating waveform. According to (2), the modulating waveform is a sinusoidal waveform and its amplitude $|s_i|$ represents the modulation index of the j^{th} cell. The control system should control s_j (j=1, 2,.. , n) in a way that the maximum power is drawn from PV arrays and the injected current to the grid remains sinusoidal.

The main challenge about the CHB based photovoltaic inverter is the control of inverter in non-uniform (or asymmetric) operating conditions. In other words, due to use of several distinct PV arrays as input sources, the system is a multi-input multi-output (MIMO) system and the control is not straightforward. When all PV arrays and H-bridge cells have identical operating conditions, the system can be considered as a simple system and the conventional control method for the single stage inverters can be utilized. However, when the irradiance levels of PV arrays or working conditions of H-bridge cells are different, it is necessary to employ a sophisticated control system in order to prevent any instability and interruption of the CHB inverter [14].

3- Control of CHB based Photovoltaic Inverter

In this paper, the presented control system in [15] is extended for a CHB inverter with an arbitrary number of H-bridge cells. In the following analysis, it is assumed that the converter is lossless and the size of dc link capacitors (C_j) are enough large. Using this assumption, one can consider that the ripple of dc links is negligible. Moreover, all dc (or average) values are demonstrated in capital letters and ac variables are shown in small letters.

a. Basis of control system

In the grid connected PV inverters, the Total Harmonic Distortion (THD) of the grid current should be less than 5% to avoid adverse effects on the other consumers and the grid [20]. Otherwise, the inverter must be stopped and isolated from the grid. To satisfy this requirement, the H-bridge cells in the CHB inverter must be prevented to incur the over modulation region. In other words, to meet the standard limits, the modulation index of each H-bridge cell should be kept lower than one [21]; otherwise it incurs to the over modulation and will generate a significant amount of harmonics and losses. Hence, in this paper, to control the amount of THD, the following condition is satisfied for each H-bridge cell.

$$|s_j| \le 1 \ , j = 1, 2,..., n \qquad (3)$$

Since the calculation of modulation index from (2) is not straightforward; therefore, a new relation for $|s_j|$ based on PV system data is extracted. To achieve this goal, it is assumed that the system is at the steady state and the injected current to the grid is sinusoidal. Since the average power of j^{th} PV array is fed to the grid by the j^{th} H-bridge cell, one can write

$$P_{array,j} = P_{H-bridge,j} \rightarrow V_{dcj} I_{PVj} = \frac{1}{2} \left| v_{hj}^1 \right| \left| i_g \right| \cos\delta \qquad (4)$$

where $|i_g|$ represents the amplitude of injected current to the grid and δ represents the phase difference between the ac terminal voltage and the grid current. Now by inserting the value of $|v_{hj}^1|$ from (2) into (4), one can obtain

$$\left| i_g \right| = \frac{2 I_{PVj}}{|s_j| \cos\delta} \qquad (5)$$

Since the total generated power by all arrays is equal to the injected power to the grid, one can write

$$P_{total} = \sum_{j=1}^{n} I_{PVj} V_{dcj} = \frac{1}{2} |v_g| . |i_g| \cos\delta \qquad (6)$$

where $|v_g|$ is the amplitude of grid voltage. Now by inserting the value of $|i_g|$ from (5) into (6) and calculation of $|S_j|$, the following result is obtained.

$$|s_j| = \frac{I_{pvj} |v_g|}{\sum_{j=1}^{n} I_{PVj} V_{dcj}} \quad for\ j = 1,2,...,n \qquad (7)$$

Equation (7) is the basis of control system to monitor the condition of H-bridge cells. If $|S_j|$ is lower than one, it means that the H-bridge cell is in the linear modulation range; otherwise it is in the over modulation and a proper action should be taken. The over modulation may happen if the generated power by PV arrays are different. In this case, the high-power cells will have a greater value for I_{pvj} and according to (7), the numerator of (7) increases and it may become greater than one. It is also worth mentioning that in contrast to (2) which needs FFT calculations for finding $|S_j|$ value, (7) calculates $|S_j|$ based on already existing PV system data (for MPPT of PV arrays) and is a much simpler approach.

b. Block diagram of control system

The modified MPPT flowchart and block diagram of control system is shown in Fig.2. As it is seen from Fig.2, the control system has three stages. First stage which is the system's control algorithm (shown as Fig.2.a) is used to perform MPPT and to calculate the dc reference voltage for H-bridge cells. Then, in second stage, the sum of reference voltages is subtracted from the total voltage of all dc links. The error signal is entered to a PI regulator and the PI output determines the amplitude of injected current to the grid, i.e., $|i_g^*|$. Next, using a phase locked loop (or PLL), a sinusoidal signal with the same frequency and phase of the grid voltage is generated and multiplied by the amplitude of reference current. The obtained reference current i_g^* is compared to the real inductor current i_g and the error signal is entered to a current controller, e.g., proportional resonant controller [22]. The output signal is summed to the grid voltage and is used as the reference ac terminal voltage for H-bridge cells. i.e., v^*_{ab}.

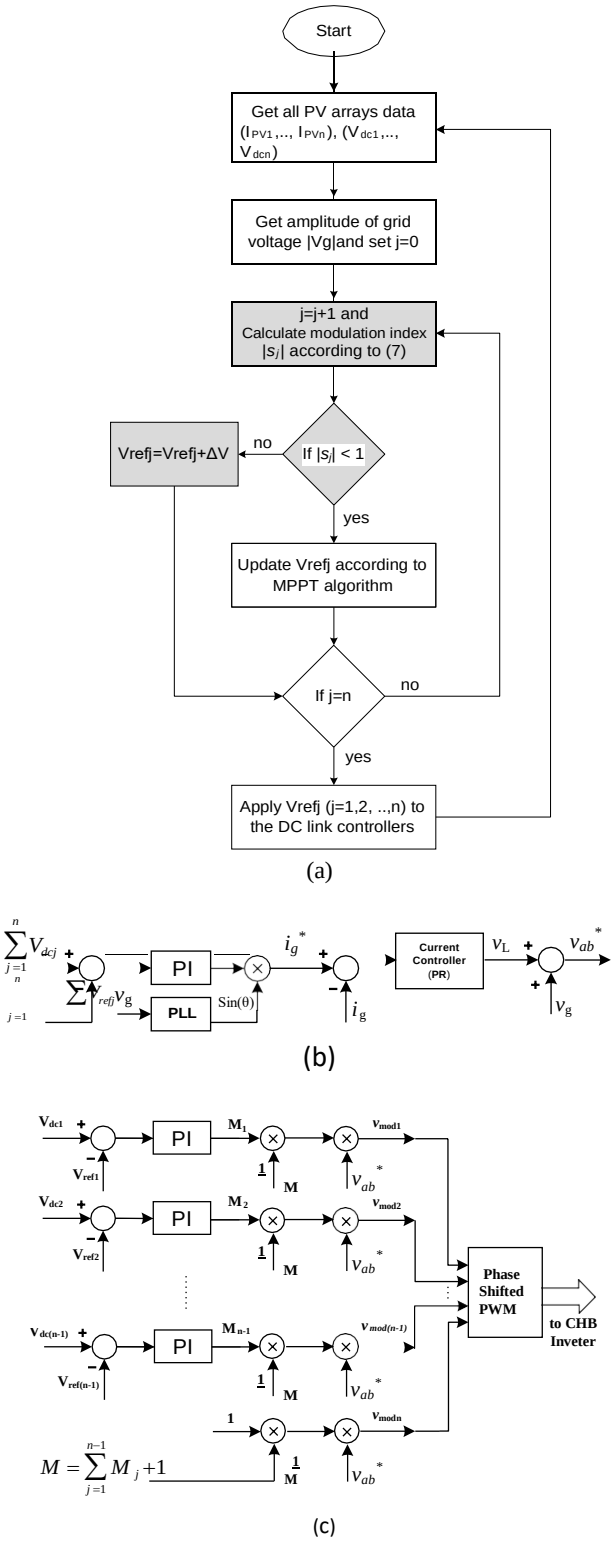

Fig. 2. Block diagram of control system, (a) flowchart of the modified MPPT, (b) grid current controller, (c) individual dc link voltage controller for each H-bridge cell

The last stage which is shown in Fig.2.c is responsible for the regulation of dc link voltages to their reference values. Since the total voltage of all dc links has been regulated to the sum of reference values in previous stage, (n-1) voltage regulators are enough for this stage. Finally, the outputs of PI regulators are divided by the sum of modulation

factors, i.e., $M = \sum_{i=1}^{n-1} M_i + 1$ and are multiplied by v_{ab}^{*} to determine the modulating functions of H-bridge cells according to (8).

$$v_{\mathrm{mod}\,j} = \frac{M_j}{\sum_{j=1}^{n-1} M_j + 1} \times v_{ab}^{*}, \quad j = 1,2,..,n-1$$
$$v_{\mathrm{mod}\,n} = \frac{1}{\sum_{j=1}^{n-1} M_j + 1} \times v_{ab}^{*} \qquad (8)$$

The modulating signals $v_{\mathrm{mod}j}$ (j=1,2,…,n) are entered to the modulation stage and are compared to the triangular carriers based on phase shift PWM (PS-PWM). This modulation technique is popular in CHB inverters and leads to equal power loss among the semiconductor switches [23]. Hence, it is selected in this paper.

One has to note that the obtained modulating signals in (8) are not precisely equal to the modulating waveforms s_j in (2). In other words, due to voltage ripple in dc links, some harmonics in the grid voltage and imperfect behavior of control system, some harmonic terms are appeared on the modulating waveforms. Hence, it is proposed to use the defined modulation indices in (2) for the control and monitoring in this paper.

c. Control of CHB inverter under non-uniform insolation conditions

During the normal operation of the CHB inverter and in steady state, the modulation index of H-bridge cells will be lower than one. However, in non-uniform insolation conditions or when PV arrays have different amounts of irradiances, the modulation indices of high-power cells may become greater than one. The H-bridge cells which incur to the over-modulation range will generate more harmonics at their ac terminal voltages and because of series connection of H-bridge cells at the ac side, the total ac voltage (the fundamental component) is highly distorted and the injected current to the grid is also affected. Thus, to prevent the above problem, the modulation index of each H-bridge cell is calculated according to (7) in each iteration of the control algorithm (see Fig. 2.a). According to the value of modulation index, two decisions are taken. If the modulation index is lower than one, the conventional perturb and observe (P&O) algorithm is employed to update the reference voltage of that cell; but, in conditions that the modulation index is greater than one, the operating point of that cell is shifted through increasing the dc link voltage as follows

$$V_{refj} = V_{refj} + \Delta V \; if \; |s_j| > 1 \qquad (9)$$

where ΔV is the step voltage for increasing the reference value and it can be selected equal or greater than the step voltage of P&O algorithm. Also the frequency of voltage update in (9) can be equal or different from the MPPT algorithm. In this paper, these two frequencies are selected equal together. This strategy helps to bring the H-bridge cell into the linear modulation range and to meet the standard limits from the THD point of view.

Based on the proposed control system, the inverter can continue its operation under non-uniform operating conditions, e.g., when the partial shading happens. This capability enhances the converter operating area and increases the availability of DG system. In other words, in contrast to conventional CHB based PV inverters which must be interrupted and isolated from the grid in asymmetric operating conditions, the new method helps to keep the converter in line and to continue the power injection.

The cost of shifting the operating point of H-bridge cells under asymmetric operating conditions is the decrease of total generated power (a few percent, depending on the asymmetry condition), but on the other hand the converter can continue its power injection to the grid.

d. Proposed voltage estimation approach for dc link voltages

In the existing control approached for the CHB based PV inverters, (2n+2) sensors, including "n" dc link voltage sensors, "n" PV current sensors, one grid voltage sensor and one grid current sensor are needed. To reduce the number of dc link voltage sensors, one may use a voltage sensor at the ac terminal of CHB inverter to measure the total ac terminal voltage, i.e., v_{ab}, before and after each transition, to estimate the dc link voltages. Due to employment of phase-shifted modulation (PS-PWM), the voltage change at the switching instant is limited to one dc link voltage level. In other words, at the transitions of v_{ab}, the switching condition of only one H-bridge cell changes and the rest H-bridge cells remain at their previous states. Now by the help of digital processor (employed for the control goal) and a fast analog-to-digital converter (ADC), it is possible to recognize the H-bridge cell which contributes to the voltage change at the switching instant. In fact, the digital processor generates the switching commands for H-bridge cells, and with a comparison between the current and previous switching states, the source of voltage change is recognized. Next, by subtracting the measured voltage of v_{ab} according to (10), the voltage of corresponding dc link is determined.

$$V_{dcj} = \left| v_{ab,t_k} - v_{ab,t_{k-1}} \right| \qquad (10)$$

where V_{dcj} represents the voltage of jth cell (or the H-bridge cell) which contributes to the voltage change. In addition, $v_{ab,tk-1}$ and $v_{ab,tk}$ are the voltage samples of ADC module, before and after voltage transition. To implement this procedure, one has to employ a fast ADC module which samples from v_{ab} with a high sampling rate (e.g., 50 kHz) and the demonstrated circuit in Fig. 3, which is shown for an arbitrary H-bridge cell in the CHB inverter.

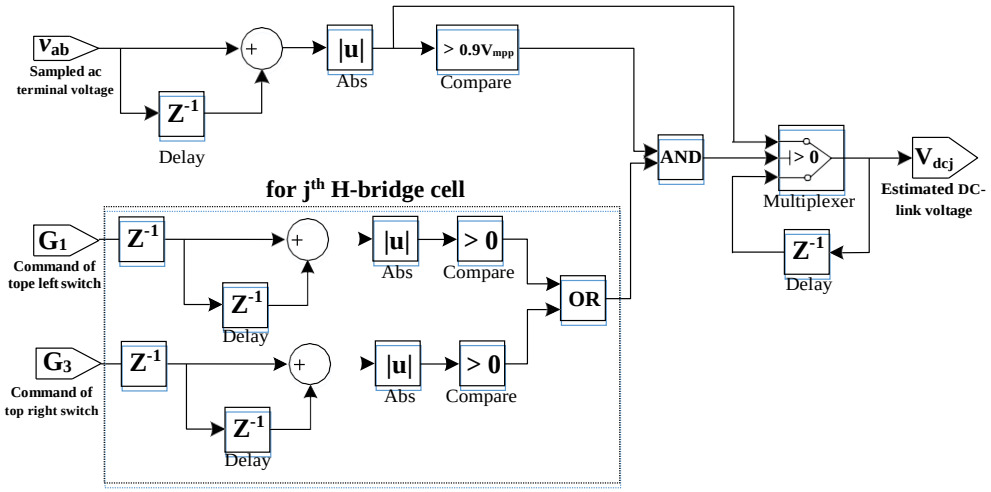

Fig. 3. Estimation of jth dc link voltage from the ac terminal voltage

Fig. 3 shows the procedure of voltage estimation for the jth dc link from the ac terminal voltage. In this figure, the block Z^{-1} is equivalent to a time-step delay of the digital controller. The corresponding gate signals of the top switches in the ^{jth} H-bridge cell are labeled by G_1 and G_3, where the bottom switches receive the complementary signals. In the positive half cycles, G_1, and in the negative half cycles, G_3, contribute to the modulation. The added delay after G_1 and G_3 represent the delay between the switching commands and the respond time of power switches. Moreover, the

multiplexer block at the last stage is used to update the voltage of dc link when a valid state is recognized; otherwise, the previous sample is used. It is worth mentioning that, due to practical considerations, the estimated dc link voltage will be valid when two conditions are met:

1) A voltage transition has occurred
2) The difference of two consecutive samples in (10) is greater than a specific limit, e.g., $0.9V_{mpp}$.

Above constraints are used to eliminate invalid voltage samples in v_{ab} or very short pulses.

4- Simulation Results

In this part, the presented control strategy is investigated on a 7-level CHB inverter with three H-bride cells (n=3). In this study, 70 W Yingli Solar modules (YGE70) are selected as PV modules. Each PV array is made of eight series connected modules and is connected to the dc link of an H-bridge cell. To simulate the behavior of PV arrays in Matlab/Simulink, the single-diode model is used. The corresponding parameters of PV arrays are shown in Table I and the system parameters are given in Table II.

Table I. PV array parameters in standard test condition (STC)

Parameter	Symbol	Value
Photo-generated current	I_{pho}	4.15 A
Diode saturation current	I_{so}	1.45 nA
Diode quality factor	A	1.11
Array series resistance	R_s	3.35 Ω
Array shunt resistance	R_p	690 Ω

Table II. Utilized parameters for system under study

Parameter		Symbol	Value
Number of H-bridge cells		N	3
Grid Voltage (rms)		Vg	230 V
Total Power at STC		P_{nom}	1680 W
Inductor value		L	4.5 mH
dc link capacitance		C	1 mF
Control system Parameters	Step voltage	ΔV	0.02 V
	Carrier frequency	f_{car}	5 kHz
	MPPT frequency	f_{mppt}	5 kHz
	Individual voltage regulators	K_p	0.002
		K_i	2
	Total voltage regulator	K_p	0.07
		K_i	5.4
	Resonant controller	K_p	120
		K_{r1}	0.1

a. Steady-state behavior of control system

The following simulation investigates the behavior of control system under heavy non-uniform insolation condition. The irradiance level of first PV arrays is assumed to be 400 W/m^2 while the second and third ones are 1000 W/m^2. Moreover, the temperature of PV arrays is assumed to be 55˚C. In this investigation, first the presented control system in [8] is applied to the CHB inverter. Then, at t=1.5 s the modified control strategy in Section 3 is applied. The corresponding grid current, PV arrays voltages, modulation indices, and the generated total power are demonstrated in Fig.4, 5, 6, 7.

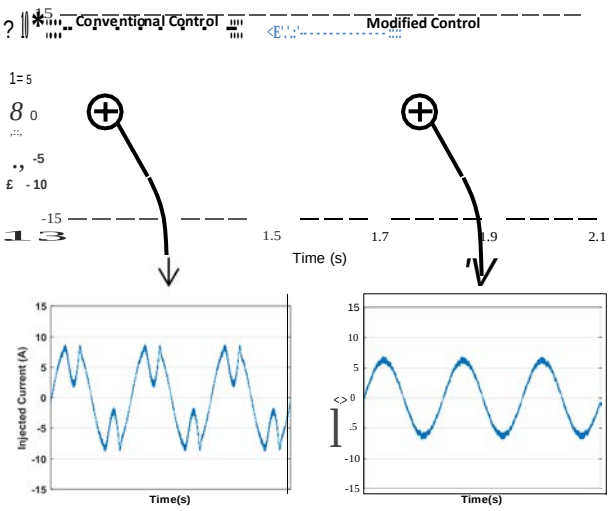

(a) (b)

Fig.4. Injected current to grid under asymmetric operating condition, (a) with the proposed controller in [8], (b) with the modified control system

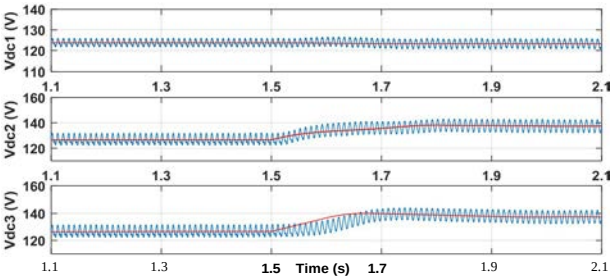

Fig.5. dc-link voltages (blue) and the reference values (red) under asymmetric operating condition when the control method in [8] and the modified one in this paper are employed.

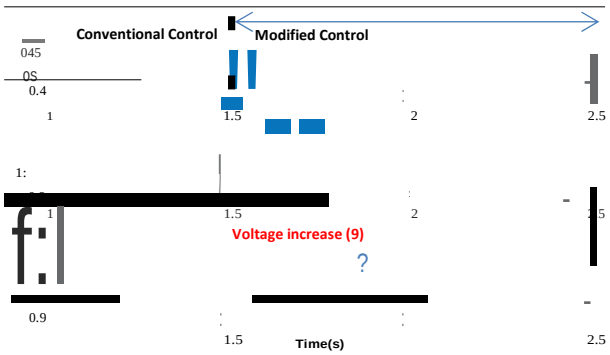

Fig.6. Defined modulation indices under asymmetric operating condition, before and after applying the modified controller

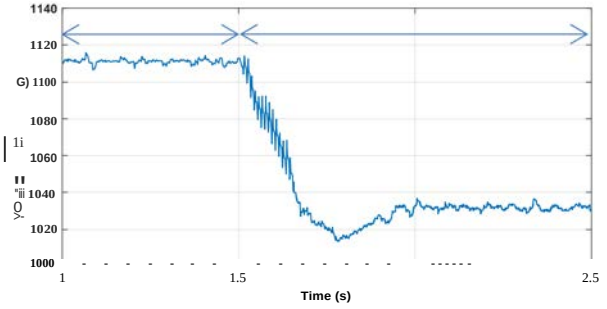

Fig.7. Total generated power, before and after applying the modified controller

According to Fig.4., the injected current to the grid is significantly distorted when the irradiance level of PV arrays are so different. However, after applying the modified control strategy at t=1.5s, the current distortion reduces

considerably and its harmonic content lies under standard limits. The control system can reach this goal through increasing the voltage of high-power PV arrays, which is shown in Fig.5. It is seen that the voltage of first PV array remains constant, while the voltage of second and third PV arrays increase to 138 V. The amount of voltage increase depends on the asymmetry of H-bridge cells. In other words, the modulation index of each H-bridge cell is checked in the MPPT algorithm and if the value is greater than one, the corresponding dc link voltage is increased based on (9) to bring the modulation index down to one. This behavior has been shown in Fig.6 for the CHB inverter. From Fig.6, it is seen that the modulation index of second and third H-bridge cells are equal to 1.1 when the conventional control is employed. But after checking modulation indices from (7) and applying the modified MPPT (gray shaded loop in Fig.2.a), the modulation indices are reduced and reach the new steady state values (i.e., one), in less than 0.3s.

As it is seen in Fig.7, for the system under investigation, the total generated power reduces from 1115 W to 1035 W (or 7.1% reduction) after applying the modified controller. One has to note that this power reduction happens when the operating condition of H-bridge cells (or PV arrays) is so different. However, it helps to keep the inverter in the network and to continue the power injection. Otherwise, due to high amount of harmonic generation, the inverter must be interrupted and isolated from the grid, if the proposed strategy is not employed.

b. Dynamic Performance of control system

The dynamic behavior of presented CHB based PV inverter depends generally on two perspectives- solar irradiance change and grid voltage variation. Hence, two different situations are simulated to verify the dynamics of CHB based PV system when the presented control system in [8] and the modified one in this paper are employed.

In the first investigation, the irradiance levels of all PV arrays are 1000 W/m^2. Then, at t=2 s, the irradiance level of first PV array reduces to 300 W/m^2 in a step-wise manner. Fig. 8.a and Fig. 8.b show the obtained results for the dc-link voltage waveforms and the injected current to the grid when the control system in [8] and the presented one in this paper are employed, respectively.

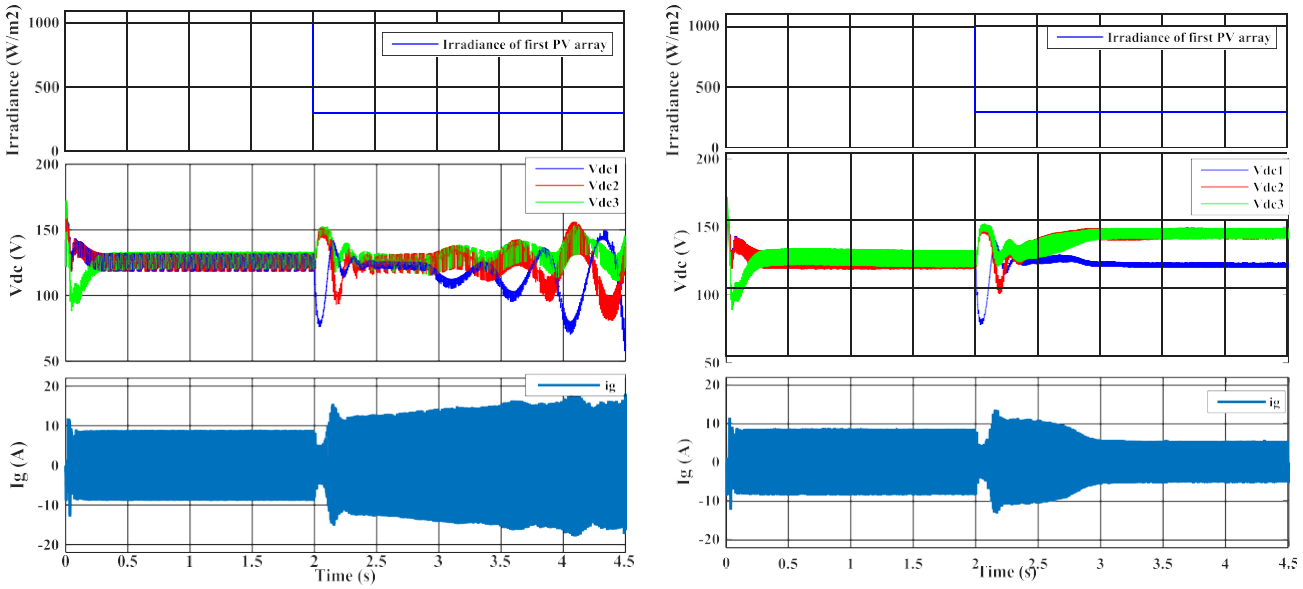

(a) (b)

Fig.8. Dynamical behavior of control system when the irradiance level of first PV array reduces from 1000 to 300 W/m^2 at t=2s: (a) behavior of control approach in [8], (b) behavior of modified control system

From Fog.8, it is evident that when the irradiance level of first PV array changes suddenly to 300 W/m^2, the control system in [8] loses the stability and both dc link voltages and the injected current to the grid are highly distorted. In contrast to [8], the modified control system well behaves in the dynamical condition and keeps the stability. The dc link voltages and the injected current to the grid reach the new steady-state condition after 0.8s. Also, it is seen that the voltage of second and third PV arrays is increased to bring the corresponding H-bridge cells back into the linear modulation range after sudden change of irradiance level.

In the second investigation, the irradiance level of first PV array is 400 W/m^2, the second and third ones are 1000 W/m^2, and the peak of grid voltage is 330 V. Then, at t=2 s, the grid voltage increases 10% in a step-wise manner. Fig. 9.a and 9.b show the dynamical behavior of dc link voltages and the injected current to the grid when the control system in [8] and the modified one in this paper are employed, respectively.

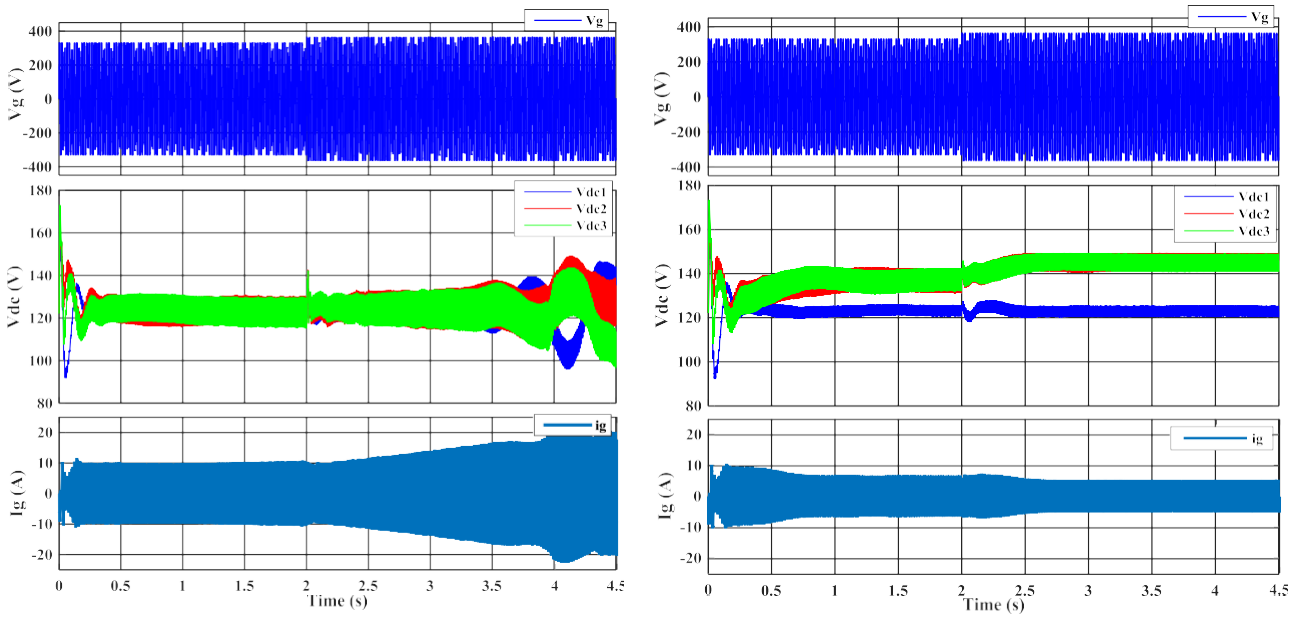

Fig.9. Dynamical behavior of control system when the grid voltage increases 10% under asymmetric operating condition at t = 2 s: (a) behavior of control approach in [8], (b) behavior of modified control system

Evaluation of Fig. 9 reveals that the presented control system in [8] fails to keep the stability when the grid voltage increases 10% in a step-wise manner. The reason is that with the increase of grid voltage, the modulation indices of second and third PV arrays incur to non-liner region and the grid current distortion increases significantly. Then, the current control is lost and the inverter operation must be interrupted. In the modified control system, however, as it is seen in Fig.9.b, the control system increases the voltages of second and third PV arrays and brings the corresponding H-bridge cells back into the linear modulation range. The transient time is less than 0.5s and both the dc link voltages and the grid current show satisfying behavior.

In the following paragraph, a comparison table is provided to evaluate the performance of different methods and the presented approach, which are suitable for CHB based PV systems.

Table III. Comparison of presented control methods for cascaded H-bridge PV systems under asymmetric operating conditions

	Reactive power compensation [12]	Reactive power control + modified LS-PWM [13]	Hybrid modulation + dP/dI control [14]	Employed approach in this paper
PV system structure	DC/DC+CHB	DC/DC+CHB	Single stage CHB	Single stage CHB
Number of sensors in a single-phase system	2N+2	2N+2	2N+2	N+3
Total efficiency	Moderate	Moderate	Good	Good
Implementation complexity	Moderate	High	High	Moderate
Stability versus heavy mismatching condition	Moderate	Very good	Very good	Good
Dynamic behavior	Moderate*	Moderate*	Good	Good
Drawback	Necessity to reactive power exchange	High computational burden and control system complexity	Sensitivity to high-frequency noise	Decrease of output power in heavy mismatching condition

*Dynamic behavior is affected by two power conversion stages (between PV arrays and the grid) and also the use of large capacitances

c. System performance in the presence of dc link voltage estimator

As it was explained in Section 3.d, using the proposed estimation approach, one can replace "n" dc-link voltage sensors with only one voltage sensor at the ac terminal and still obtains satisfactory results. The effectiveness of the estimation method is verified by following simulations. Here, the test condition is same as the dynamical condition in Fig.9.b, where the irradiance level of first PV array is 400 W/m^2, the second and third ones are 1000 W/m^2, and the peak of grid voltage is 330 V. Then, at t=2 s, the grid voltage increases 10% in a step-wise manner. The following results in Fig.10.a and Fig.10.b show a zoomed view of dc-link voltages and the grid current when dc-link voltage sensors are employed and when the proposed estimation method is applied, respectively.

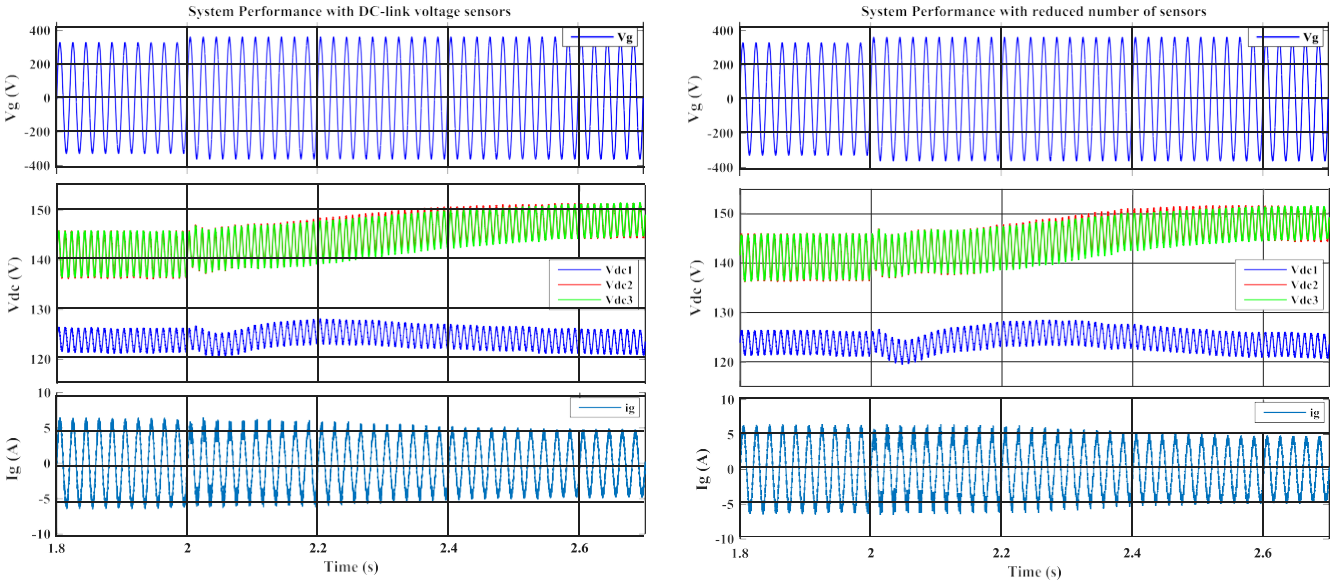

(a) (b)

Fig.10. Investigation of control system performance in dynamic condition: (a) in the presence of dc-link voltage sensors, (b) when the proposed estimation approach is employed

Comparing the obtained results in the presence of dc-link voltage sensors and with the estimation approach confirm the correct behavior of new estimator. There is only a small difference in dynamical conditions, due to reduced number of data when the estimation approach is applied. This fact can be observed in Fig.11, where the estimated voltages are compared to real ones in three different operating points, i.e., before voltage swell, during transient time, and after voltage swell. Also, one should note that in Fig.11, due to non-uniform distribution of irradiances, the first cell contributes in the modulation more than 2nd and 3rd ones and hence it has more points of estimations.

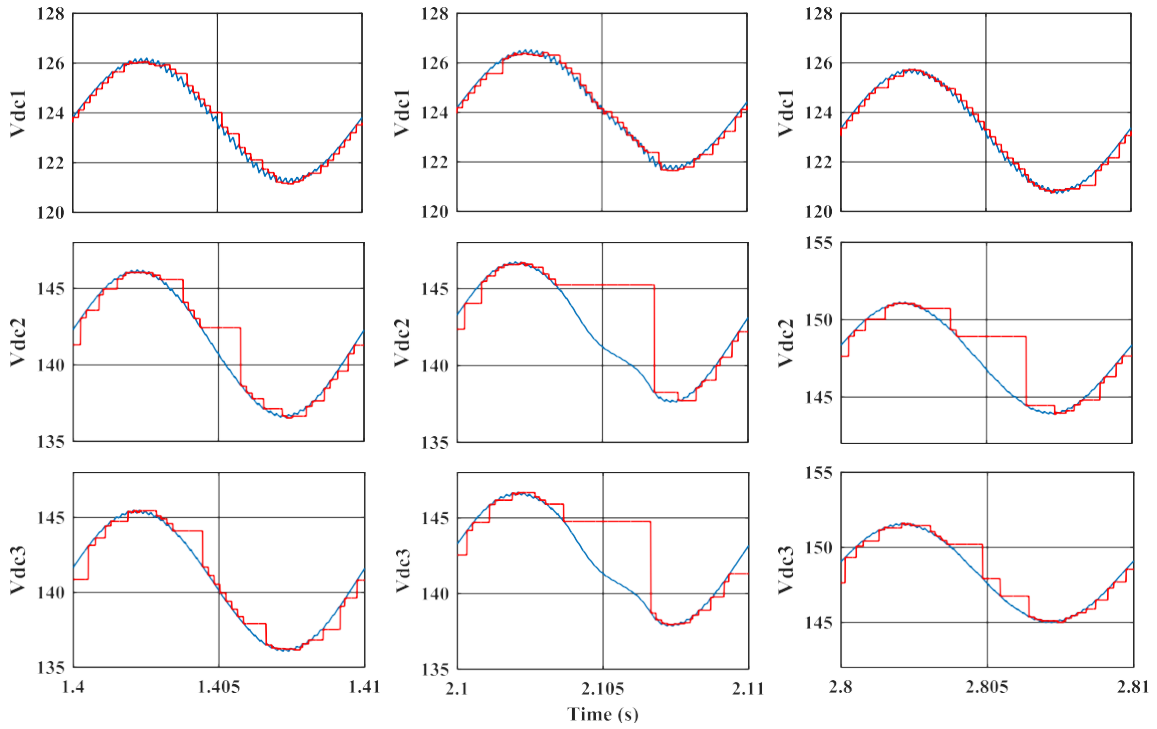

Fig.11. Evaluation of voltage estimation method at three different periods of Fig10.b: Blue: Measured dc-link voltages, Red: Estimated dc-link voltages (that the control system works based on them)

5- Hardware-in-the-loop simulation of the CHB Inverter

In this part, first the hardware-in-the-loop (HIL) real-time simulation of the photovoltaic system is explained. In fact, using HIL simulation, the cost and complexity of experimental investigation reduces significantly. Moreover, fast prototyping of PV inverters is achieved.

At first, the control system is implemented and programmed according to the flowchart of Fig.2. In this investigation, TMSF28335 digital signal processor is used as the main processor of control system. All the control functions are written by C language and programmed to the DSP. The control circuit is connected to the OPAL-RT hardware (i.e., OP4510) by the provided I/O ports at the back of OP4510 (see Fig.12).

The next step is the modelling of PV arrays and the CHB inverter in the RT-LAB environment. The RT-LAB software is linked to the Matlab/Simulink program and allows building the photovoltaic system (e.g., PV arrays and the CHB inverter) in the Simulink environment. Using the added toolboxes of RT-LAB to the Matlab/Simulink, one can make necessary connections between the real-time simulator and the external controller. In addition, using the OpComm block of RT-LAB, one can separate the computation subsystem from the user-interface in the Simulink environment. The computation subsystem will be compiled and loaded to the OPAL-RT hardware and the user-

interface subsystem will allow the user to adjust the variables in the host PC during the real-time simulation. For example, the irradiance level, temperature and grid voltage can be adjusted during the real-time simulation by the user-interface.

Fig.13 shows the block diagram of HIL implementation of CHB inverter. As it can be seen, the behavior of PV arrays and CHB inverter will be simulated by the OPAL-RT hardware and the external controller will be connected to the OPAL-RT using the AnalogIn and AnalogOut ports. The PV arrays data, grid voltage and grid current will be sent to the DSP controller and the generated PWM gate signals will be returned to the OPAL-RT hardware.

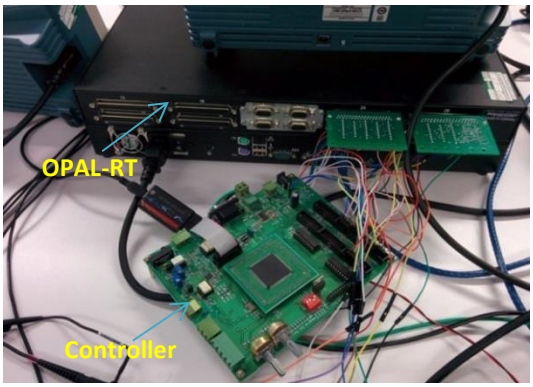

Fig.12. Picture of experimental setup for the real-time simulation

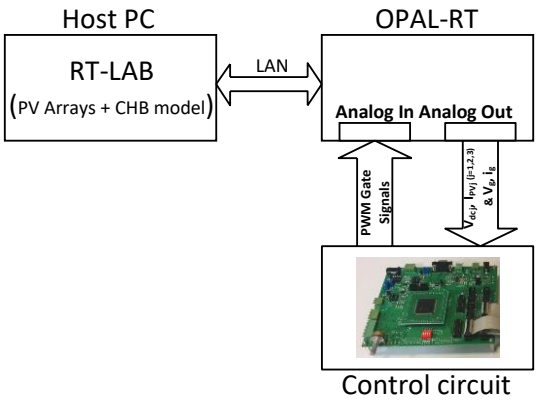

Fig.13. Block diagram of hardware-in-the-loop simulation of photovoltaic system

The system parameters in the real-time simulation are selected same as the case study in Section 4. The control system parameters are also selected similar to Table II. The only difference is related to insertion of some limiters at the output of PI controllers of DSP controller. In the following, to demonstrate the electric signals, they are defined as output signals in the RT-LAB environment and then are measured by an oscilloscope. It is also worth mentioning that the time step of real-time simulation is set to 10 µs. Selecting a greater value for the time step will cause more distortion on the obtained results.

Similar to the case study of Section 4, the irradiance level of first PV array is set to 400 W/m^2 while the irradiance level of second and third PV arrays are 1000 W/m^2. In addition, the temperature of all arrays is assumed to be 55˚C. The presented control system in [8] is applied to the CHB inverter at first; then, the modified control system is applied to the CHB inverter. The corresponding results are demonstrated in Figures 14 to 17.

Fig.14 demonstrates the dc link voltages and the grid current, before and after applying the modified control system. A zoomed view of grid current and grid voltage are shown in Fig.15 and Fig.16, where the first one is related to the steady state behavior of the conventional controller and the latter to the modified controller.

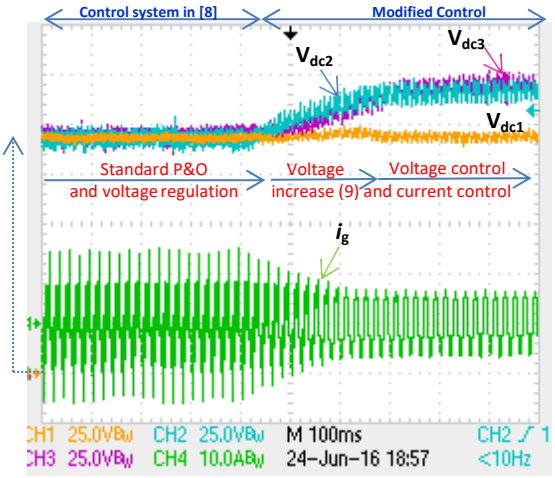

Fig.14. Dc link voltages and grid current under asymmetric operating condition with the conventional and modified controller

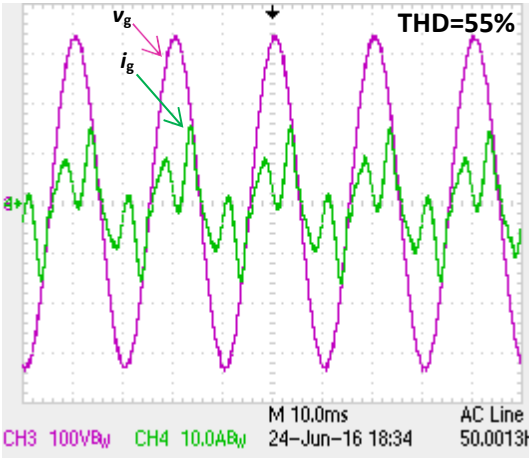

Fig.15. Grid voltage and current under asymmetric operating condition with the presented controller in [8] (Ch3: 100V/div, Ch4: 10 A/div)

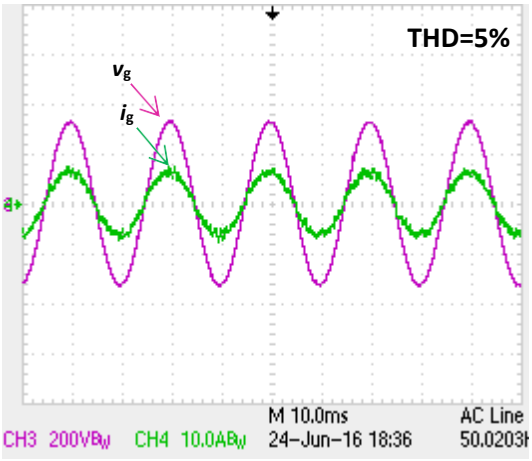

Fig.16. Grid voltage and current under asymmetric operating condition with the modified controller (Ch3: 200V/div, Ch4: 10 A/div)

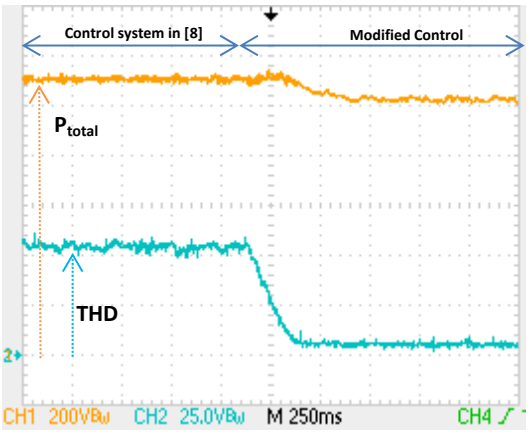

Fig.17. Total generated power (top, 200 W/division) and the corresponding THD of injected current (bottom, 25% per division)

According to Fig.14, the voltage of first dc link remains constant while the voltage of second and third dc links increase from 120 V to 140 V after applying the modified control system. This strategy helps to decrease the THD of grid current to the standard limits which is confirmed by comparison of the grid current in Fig.15 and Fig.16.

The last figure shows the total generated power and THD of injected current in the presence of conventional controller and modified control system, under asymmetric operating condition. As it is seen from Fig.17, the total generated power reduces from 1100 W to 1020 W after applying the modified controller. Moreover, the THD of injected current reduces from 55% to 5% which justifies the application of modified control system in the control of CHB inverters. Otherwise, the CHB inverter must be interrupted and isolated from the grid due to high amount of harmonics generation and losses.

Small differences among the results of simulated system in Section 4 and the HIL simulation in Section 5 are related to differences of two control systems. For example, in DSP based control system, some additional limiters have been added to the controllers (to prevent overflow of counters) which increase the non-linearity of control system. This fact can be confirmed by comparison of Fig.4.a and Fig.15, where the THD of current is 45% in the first one and 55% in the second one.

6- Conclusions

In this paper, the employment of cascaded H-bridge inverter for photovoltaic applications was explained. To guarantee the correct operation of CHB inverter in non-uniform (or asymmetric) operating conditions, a modified MPPT algorithm was employed. In the modified algorithm, the value of modulating indices of H-bridge cells are calculated based on the presented formula in (7) and then the reference voltages of PV arrays are increased if they are in the over modulation region. This idea helps to bring the H-bridge cells back into the linear modulation range and reduce the THD of injected current to the grid. The dynamic performance of control system was evaluated through simulations and compared to the conventional approach. Also, a new voltage estimation approach was proposed to reduce the number of voltage sensors in the control system. The control system then was verified using the off-line and real-time hardware-in-the-loop simulations. The structure of HIL implementation of photovoltaic system was explained in detail and the obtained results were demonstrated.

References

[1] J. T. Bialasiewicz, "Renewable Energy Systems with Photovoltaic Power Generators: Operation and Modeling," *IEEE Trans. Ind. Electron.*, vol. 55, no.7, pp. 2752-2758, Jul. 2008.

[2] S. B. Kjaer, J. K. Pedersen, and F. Blaabjerg, "A review of single-phase grid connected inverters for photovoltaic modules," *IEEE Trans. Ind. Appl*., vol.41, no. 5, pp. 1292-1306, Sep./Oct. 2005.

[3] M.R. Islam, Y. Guo, and J. Zhu, "A multilevel medium-voltage inverter for step-up-transformer-less grid connection of photovoltaic power plants," *IEEE J. Photovolt.*, vol. 4, no. 3, pp. 881-889, May 2014.

[4] S. Kouro, J.I. Leon, D. Vinnikov, and L.G. Franquelo, "Grid-connected photovoltaic systems: an overview of recent research and emerging PV converter technology," *IEEE Ind. Electron. Mag*., vol.9, no.1, pp. 47-61. , Mar. 2015.

[5] L. Liming L. Liu, L. Hui, X. Yaosuo; and L. Wenxin , "Reactive power compensation and optimization strategy for grid-interactive cascaded photovoltaic systems," *IEEE Trans. Power Electron.*, vol. 30, no.1, pp. 188-202, Jan. 2015.

[6] B. Xiao, L. Hang, J. Mei, C. Riley, L. Tolbert, and B. Ozpineci, "Modular cascaded H-bridge multilevel PV inverter with distributed MPPT for grid-connected applications", *IEEE Trans. Ind. Appl*., vol.51, no.2, pp. 1722-1731, Mar. 2015.

[7] C. Cecati, F. Ciancetta, and P. Siano, "A multilevel inverter for photovoltaic systems with fuzzy logic control," *IEEE Trans. Ind. Electron*., vol. 57, no. 12, pp. 4115–4125, Dec. 2010.

[8] E. Villanueva, P. Correa, J. Rodriguez, and M. Pacas, "Control of a single-phase cascaded H-bridge multilevel inverter for grid-connected photovoltaic systems," *IEEE Trans. Ind. Electron.*, vol. 56, no. 11, pp. 4399-4406,Aug. 2009.

[9] S. Kouro, B. Wu, A. Moya, E. Villanueva, P. Correa, and J. Rodriguez, "Control of a cascaded H-bridge multilevel converter for grid connection of photovoltaic systems," *35th Annual Conference on Industrial Electronics* (IECON '09), pp. 3976-3982, 2009.

[10] G. Farivar, B. Hredzak, and V. Agelidis, "A dc-side sensorless cascaded H-bridge multilevel converter based photovoltaic system," *IEEE Trans. Ind. Electron*, early access.

[11] M. Rezaei, H. Iman-Eini, and S. Farhangi, "Grid-connected photovoltaic system based on a cascaded H-bridge inverter," *Journal of Power Electronics*, vol. 12, no. 4, July 2012.

[12] L. Liu, H. Li, Y. Xue, and W. Liu, "Decoupled Active and Reactive Power Control for Large Scale Grid-Connected Photovoltaic Systems Using Cascaded Modular Multilevel Converters," *IEEE Trans. Power Electron.*, vol. 30, no. 1, pp. 176-187, Jan. 2015.

[13] L. Liu and et al, "A Coordinated Compensation Strategy for Module-Mismatch of CHB-PV Systems Based on Improved LS-PWM and Reactive Power Injection" to be appear *in IEEE Transactions on Industrial Electronics*.

[14] M. Miranbeigi, H. Iman-Eini, "Hybrid Modulation Technique for Grid-Connected Cascaded Photovoltaic Systems," *IEEE Trans. Ind. Electron*., vol. 63, no. 12, pp 7843–7853, Jun. 2016.

[15] A. Eskandari V. Javadian, H. Iman-Eini, and M. Yadollahi, "Stable operation of grid connected Cascaded H-Bridge inverter under unbalanced insolation conditions," *3rd International Conference on Electric Power and Energy Conversion Systems*, pp. 1-6, Oct. 2013.

[16] H. Iman-Eini, S. Bacha, D. Frey, "Improved control algorithm for grid-connected cascaded H-bridge photovoltaic inverters under asymmetric operating conditions," *IET Power Electronics*, vol. 11, no. 3, pp. 407-415, Mar. 2018.

[17] Y. Mahmoud, and E. F. El-Saadany, "Fast Power-Peaks Estimator for Partially Shaded PV Systems," *IEEE Trans. Energy Convers.*, vol. 31, no. 1, pp. 206–217, Mar. 2016.

[18] R. Selvamuthukumaran, and R. Gupta, "Rapid prototyping of power electronics converters for photovoltaic system application using Xilinx System Generator," *IET Power Electron.*, vol. 7, no.9, pp. 2269-2278, Sep. 2014.

[19] X. Zhang, F. Zheng, J. Zhang, and J. Huang, "Study on the Grid Adaptability Test for Photovoltaic Inverter Based on RT-LAB Simulator," *International Conference on Renewable Power Generation*, pp. 1-5, Oct. 2015.

[20] Y. Yang, K. Zhou, and F. Blaabjerg, "Current harmonics from single-phase grid-connected inverters, examination and suppression," *IEEE J. Emerg. Sel. Topics Power Electron.*, vol.4, no. 1, pp. 221-233, Mar.2016.

[21] K. Zhou and D. Wang, "Relationship between space-vector modulation and three-phase carrier-based PWM: a comprehensive analysis," *IEEE Trans. Ind. Electron.*, vol. 49, no.1, pp. 186-196, Feb. 2002.

[22] H. cha, T.K. Vu and J.E. Kim, "Design and Control of Proportional- Resonant Controller based on Photovoltaic Power Conditioning System", IEEE *Energy Conversion Congress and Exposition*, pp. 2198-2205, 2009.

[23] M. Malinowski, K. Gopakumar, J. Rodriguez, and M.A. Perez, "A survey on cascaded multilevel inverters," *IEEE Trans. Ind. Electron*., vol. 57, no. 7, pp. 2197–2206, Jul. 2010.